THE JOURNAL OF PHYSICAL CHEMISTRY Letters

pubs.acs.org/JPCL

High-Throughput Measurement of the Seebeck Coefficient and the Electrical Conductivity of Lithographically Patterned Polycrystalline PbTe Nanowires

Yongan Yang, David K. Taggart, Ming H. Cheng, John C. Hemminger, and Reginald M. Penner*

Department of Chemistry, University of California, Irvine, California 92697-2025, United States

ABSTRACT A high-throughput method for measuring the Seebeck coefficient, S, and the electrical conductivity, σ, of lithographically patterned nanowire arrays is described. Our method involves the microfabrication of two heaters and two Ag/Ni thermocouples, literally on top of an array of polycrystalline PbTe nanowires synthesized on a Si_3N_4 wafer using the lithographically patterned nanowire electrodeposition (LPNE) method. This strategy eliminates the transfer and manipulation of nanowires as a prerequisite for carrying out measurements on these wires of thermoelectric metrics. With these devices, we have measured the influence of the thermal annealing temperature on the thermoelectric properties of nine arrays of 60 nm $\times$200 nm $\times$ 200 μm PbTe nanowires, and we find that at an optimum annealing temperature of 453 K, the S at 300 K is increased from -41 μV/K for unannealed wires to -479 μV/K, 80% larger in magnitude than the S (-260 μV/K) of bulk PbTe.

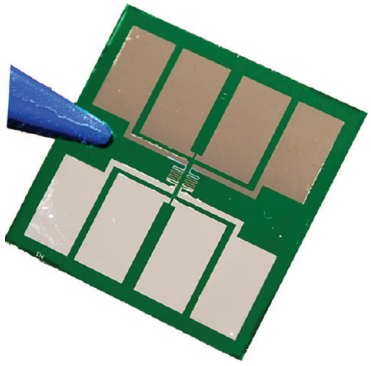

SECTION Nanoparticles and Nanostructures

The efficiency of a thermoelectric element is determined by its dimensionless figure-of-merit, ZT[1]

$$ZT = \frac{\sigma T S^2}{\kappa} \quad (1)$$

where σ is the electrical conductivity of the thermoelement, S is the Seebeck coefficient, κ is the thermal conductivity, and T is the mean absolute temperature. Lead telluride (PbTe), a semiconductor with a band gap of 0.31 eV (direct) at 300 K,[2,3] is among the most efficient bulk thermoelectric materials with a ZT of 0.45 at 300 K and 0.85 at 700 K.[4] Reducing the diameter of nanowires composed of thermoelectric materials such as PbTe to the nanometer scale is predicted to increase S[5,6] and depress κ,[7−10] both of these effects leading, via eq 1, to an elevation in ZT.

Testing these predictions presents two experimental challenges. First, nanowires of candidate thermoelectric materials must be synthesized with control of wire diameter and length, crystallinity and crystal structure, and doping. Second, one or more of these nanowires must be incorporated into devices that enable the measurement of S, σ, and κ. A realization of the potential for nanowire-based thermoelectrics requires integrating nanowire synthesis and the measurement of S, σ, and κ in a feedback loop. This integration of nanowire synthesis with measurement of S, σ, and κ has already occurred in a few laboratories. Shi and co-workers have measured all three of these metrics for electrodeposited Bi_2Te_3 nanowires[11,12] and for InSb nanowires prepared by vapor−liquid−solid (VLS) growth.[13−15] Lee and co-workers[16,17] have measured κ for single-crystalline PbTe nanowires as a function of the wire diameter. Silicon nanowires have been prepared and their thermoelectric properties have been measured by two research groups.[18,19] These two papers are the first to demonstrate an elevation of ZT for nanowires above the bulk value. The small number of references here testifies to the difficulty of incorporating nanowires prepared by hydrothermal synthesis,[20−22] chemical vapor transfer,[16,23] molecular beam epitaxy,[24,25] or templated electrodeposition[26−30] that, in all these cases, are tens of micrometers in total length into devices while achieving low-resistance ohmic electrical contacts to these nanowires.

We have recently developed a wafer-scale method for patterning polycrystalline PbTe nanowires onto dielectrics called lithographically patterned nanowire electrodeposition (LPNE).[30,31] Here, we describe how LPNE can be used to "pre-position" an array of PbTe nanowires on a Si_3N_4 wafer prior to the microfabrication of a device that enables a measurement of S, σ, and parameters derived from them. This approach eliminates the requirement for manipulating free-standing nanowires while also facilitating the measurement of S for arrays of ~200 size-similar nanowires prepared, in place, in a single synthesis operation. The total time required to synthesize

Received Date: August 11, 2010
Accepted Date: September 21, 2010
Published on Web Date: September 24, 2010

© 2010 American Chemical Society

DOI: 10.1021/jz101128d | *J. Phys. Chem. Lett.* **2010**, *1*, 3004–3011

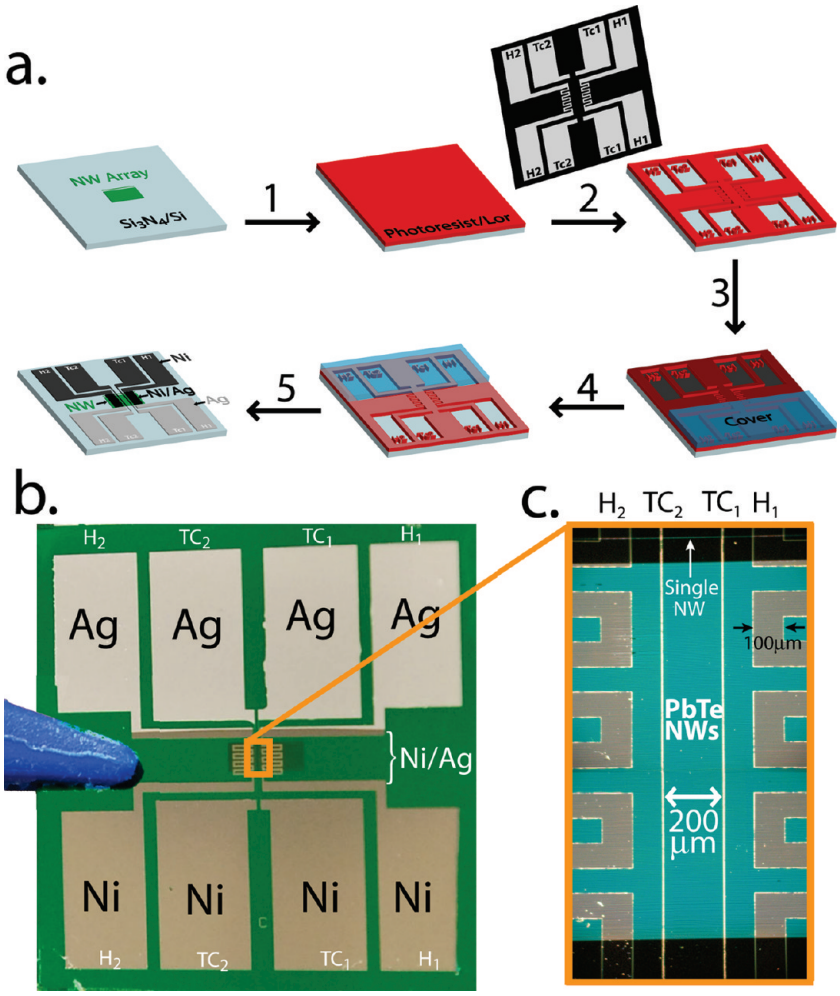

Figure 1. A device for high-throughput measurement of S and σ for nanowire arrays. (a) Five-step process flow for the fabrication, atop an array of PbTe nanowires (green), of two meander heaters and two Ag/Ni thermocouples. Step 1: A photoresist layer (Shipley 1808) is added. Step 2: Photoresist is photopatterned to enable the fabrication of heaters, thermocouples, and electrical contacts in steps 3 and 4. Step 3: Nickel is evaporated onto approximately one-half of the exposed pattern. Step 4: Silver is evaporated onto the other half. Step 5: The region at the center of the wafer, occupied by the heaters and the thermocouples, receives both nickel and silver evaporated layers in sequence. (b,c) Photograph (b) and micrograph (c) of the completed device. The blue region in (c) is an array of 60 nm × 200 nm PbTe nanowires oriented horizontally. The two vertical lines near the center of image (c), spaced by 200 μm, are the Ag/Ni thermocouples, which are 4 μm in width. Finally, a single "orphaned" nanowire that is separated laterally from the nanowire array by ~100μm is shown at the top.

PbTe nanowires arrays, construct these devices, and acquire temperature-dependent measurements of S and σ at 11 temperature points between 200 and 300 K was ~36 h for the first sample and 24 h for subsequent samples prepared in the same synthesis operation. The S measured in this way should provide an accurate representation of the mean S of nanowires prepared in a single LPNE operation, which, therefore, are narrowly dispersed in width, height, and chemical composition. Using this approach, we report here measurements of S and σ for nine 60 nm × 200 nm PbTe nanowire arrays that have been subjected to thermal annealing treatments at three temperatures.

A microfabricated device for measuring S and σ was prepared starting with an array of ~200 PbTe nanowires synthesized using the LPNE method, as previously described.[30,31] This five-step process (Figure 1a) permitted two meander heaters and two thermocouples to be deposited on top of this array (Figure 1b), providing the ability to heat the array from either side while simultaneously measuring the mean temperature and the difference in temperature across a 200 μm length segment (Figure 1c). A high thermal conductivity of the support for the device is important because the mean temperature of the nanowires is controlled by thermostatting a brass stage upon which this device is supported within a vacuum shroud, and expeditious measurements of S and σ across a range of temperatures require that the device remain in rapid thermal equilibrium. For this reason, wafers consisting of an electrically insulating silicon nitride (Si_3N_4) layer (thickness = 400 nm) on [100] silicon (thickness = 670 μm) was used as the support in preference to glass because the thermal conductivity is more than 100 times higher. In this device configuration, the electrical contacts employed for measurement of the Seebeck voltage, V_s are the same as those of the two thermocouples (TC_1 and TC_2) involved in the measurement of the temperature, and this confers the advantage that the temperature measurement

© 2010 American Chemical Society

DOI: 10.1021/jz101128d | J. Phys. Chem. Lett. 2010, 1, 3004–3011

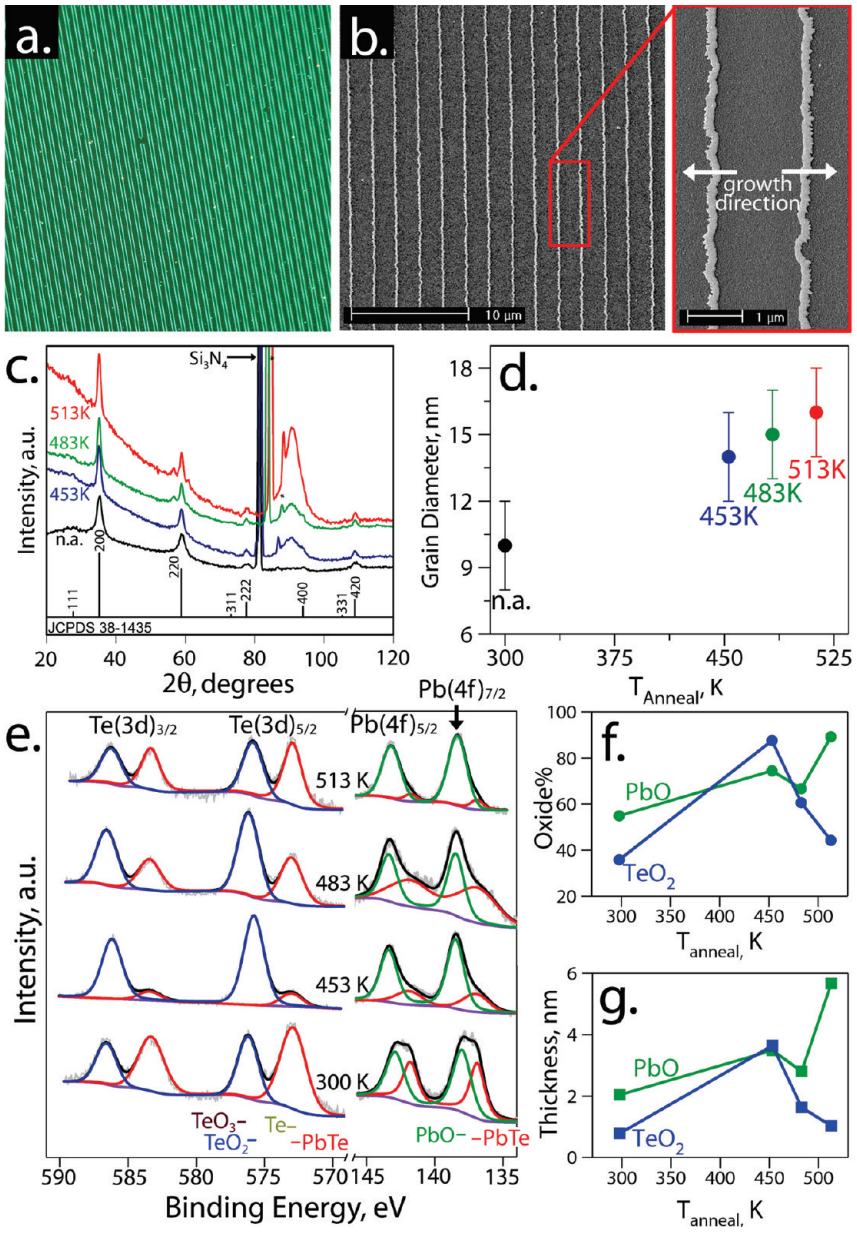

Figure 2. Characterization of as-prepared and thermally annealed PbTe nanowires. (a) Optical micrograph (150 μm × 150 μm) of a PbTe array in which 40 nm × 200 nm PbTe wires with lengths of a millimeter or more, prepared by LPNE, have been deposited at 2 μm pitch. (b) Scanning electron micrographs (SEM) of 60 nm × 200 nm PbTe nanowires. (c) Grazing incidence X-ray powder diffraction (GIXRD) of PbTe nanowire arrays. Diffraction patterns are shown for arrays that were as-prepared (not annealed, n.a.) and for which annealing was carried out for 0.5 h at the indicated temperature. (d) Grain diameter, d, estimated using the Scherrer equation and determined from the width of the 200 reflection. Error bars indicating $\pm 1\sigma$ indicate the sample-to-sample variability of d. (e) X-ray photoelectron spectra (XPS) of PbTe nanowire arrays showing the Te(3d) and Pb(4f) spectral regions for nanowires subjected to same four annealing protocols. (f) Fraction in % of the total signal for Pb and Te attributable to oxide (see text) plotted as a function of the annealing temperature. (g) Estimated thickness of the oxide (either PbO or TeO_2) plotted as a function of the annealing temperature.

occurs precisely at the point of electrical contact to the nanowires, something that is not easily achievable for temperature measurements carried out using a resistive temperature detector (RTD).[18,19]

PbTe nanowires prepared on Si_3N_4/Si wafers were indistinguishable from PbTe nanowires synthesized earlier on glass[30,31] both in terms of the morphology of these nanowires (Figure 2a,b) and in terms of their structure and chemical composition revealed by GIXRD (Figure 2c) and XPS (Figure 2e). A bright-field optical image of 40 nm × 200 nm PbTe nanowires, deposited at 2 μm pitch, reveals the existence of defects that disrupt conduction in just 3 of the ~70 nanowires shown in this region, despite the fact that the LPNE fabrication process was carried out in unfiltered laboratory ambient air. The length of these nanowires is limited only by the dimensions of the photomask (Figure 1a). SEM images of

© 2010 American Chemical Society

DOI: 10.1021/jz101128d | J. Phys. Chem. Lett. 2010, 1, 3004–3011

Table 1. Summary of Measured Seebeck Coefficient and Electrical Conductivity at 300 K for Bulk and Nanostructured PbTe

sample[a]	thermal treatment	grain diameter[b]	size[c]	S (μV/K)	σ (S/m)	$S^2\sigma$ (μW/mK^2)	ref[d]
NW film	353 K × 12 h	SC	30 nm × 100 μm	−628	133	52	Guo[22]
NW film	353 K × 12 h	SC	20−40 nm × 100 μm	−307	273	26	Guo[21]
NW film	none	SC	10−30 nm × 3 μm	410	2000	336	Yan[52]
NR film	none	SC	66 nm × 0.7 μm	−263	−	−	Ramanath[53]
NC film	573 K × 2 h	SC	30−60 nm	−451	28	5.7	Hu[54]
single NW	none	SC	60 nm × 2 μm × 2 μm	−72	0.44	0.0023	Lee[16]
single NW	none	SC	83 nm × 2 μm	−	10	−	Yang[23]
bulk	618 K × 162−228 h	30−60 nm	−	−174− −508	500 − 2 × 10^4	122−648	Heremans[55]
bulk	−	SC	−	−265	2.7 × 10^5	1900	Heremans[55]
NW array	none	10 ± 2	60 nm ×200 nm ×200 μm	−41	8100 ± 1800	14	this work
NW array	453 K × 30 m	14 ± 2	same	−479	43 ± 9	9.8	this work
NW array	483 K × 30 m	15 ± 2	same	−445	63 ± 34	13	this work
NW array	513 K × 30 m	16 ± 2	same	−366	35 ± 19	4.7	this work

[a] Abbreviations: NW = nanowire, NR = nanorod, NC = nanocube. [b] SC = single crystalline. [c] Diameter × length or width × height × length. [d] Corresponding author.

an array of PbTe nanowires (Figure 2b) shows the well-controlled width and two-dimensional trajectory on the substrate, which are desirable for thermoelectric property measurements.

For PbTe nanowires subjected to thermal annealing, two processing steps preceded the scheme shown in Figure 1a. First, freshly synthesized PbTe nanowires were encapsulated in a thin layer of Lift Off Resist (Microchem Lor 5A). Then, the encapsulated nanowires were heated in flowing N_2 at an annealing temperature, T_{anneal}, of 453 K (or 483 or 513 K) for 30 min. The purpose of the Lor 5A was to prevent morphology changes to the PbTe nanowires induced by grain growth that might cause wire breakage. After thermal annealing, a thin layer of photoresist (Shipley 1808) was spin-coated on the top of the Lor layer, and then, the sample was baked at 363 K for an additional 30 min prior to photopatterning, as shown in Figure 1a. Unlike photoresist, Lor is not photoreactive, but it is rapidly removed by the developer used for photoresist processing. The use of the Lor 5A preserved the morphology of the unannealed PbTe nanowires (data not shown), but GIXRD patterns for the annealed nanowires (Figure 2c) reveal line narrowing consistent with grain growth. The line width of the (200) reflection was used in conjunction with the Scherrer equation[32] to estimate the grain diameter, d, which increased linearly with T_{anneal} from 10 nm for unannealed PbTe to 16 nm for PbTe wires annealed at 513 K (Figure 2d).

In addition to inducing grain growth, thermal annealing also caused changes to the surface chemical composition of PbTe nanowires revealed by XPS (Figure 2e). Deconvolution curve fitting was used to analyze the chemical states of the Pb and Te present at the nanowire surface for samples annealed for 30 min at each T_{anneal}. For Te(3d), two distinct chemical states, each represented by a doublet of peaks,[33] were present in each spectrum. For the $3d_{5/2}$ peak, the lower binding energy (BE) component at 573.0 eV (red) is assigned to PbTe,[34−36] and the higher BE component at 576.0 eV (blue) is assigned to TeO_2. An analogous situation exists with the lead where, again, a pair of spin−orbit-coupled doublets are observed for all four samples. For these spectra, the lower-energy $4f_{7/2}$ component with a BE of 136.9 eV is assigned to PbTe,[34−36] and the higher-energy component with BE of 138.1 eV (green) is assigned to PbO.[37] The fraction of the observed Pb and Te present as PbO and TeO_2 is plotted versus the annealing temperature in Figure 2f. The presence of oxide in these spectra is not surprising since PbTe nanowires are exposed to laboratory air for approximately 30 min prior to transfer to the vacuum environment in which these XPS spectra were acquired. This air exposure is approximately the same as was experienced by nanowires during the fabrication steps required for preparation of the device shown in Figure 1. On the basis of the layered oxide structure model suggested by Bando et al.[38,39] and the inelastic mean-free paths of the photoelectrons,[40] the equivalent thickness of the oxide layers was also estimated as a function of T_{anneal} (Figure 2g). Plots of the thickness of the oxide layers versus T_{anneal}, both PbO and TeO_2, have maxima at 453 K, and these oxide layers are progressively reduced in thickness at 483 and 513 K. Additional experiments will be required to understand this evolution with temperature. However, one possible explanation for the complex behavior seen in Figures 2f,g is the following; the volatility of TeO_2 is considerably higher than that of PbO at temperatures above 450 K.[41,42] If the Lor layer has some permeability to residual O_2 and water vapor, then wire oxidation can occur, and the preferential loss of TeO_2 relative to PbO through the Lor layer, or the dissolution of TeO_2 into the Lor layer, might be expected to occur at 483 and 513 K. It is also possible that decomposition of the Lor, a poly(methylglutarimide), supplies the oxygen required for nanowire oxidation and that this process is optimized at 453 K. Previously,[30] we have shown that the formation of oxides on PbTe nanowire surfaces is associated with a reduction in σ, and we observe a similar depression of σ here (Table 1). The maximum thickness of the oxide at T_{anneal} = 453 K also coincides with the maximum Seebeck coefficient measured in this study. Thus, the presence of the oxide layer and its thickness may have a complex influence on the thermoelectric performance of these nanowires, and further study will be required to fully understand its effect.

© 2010 American Chemical Society

DOI: 10.1021/jz101128d | J. Phys. Chem. Lett. 2010, 1, 3004–3011

The measurement of S was accomplished by placing the device shown in Figure 1 on the brass stage of a vacuum cryostat (base pressure = 5×10^{-6} Torr) that permitted the mean temperature to be varied from 200 to 300 K in 10 K intervals. At each temperature within this interval, one of the heaters was powered by a constant dc current, the temperatures at the two TCs (calibrated prior to use) were simultaneously measured, and the V_s developed between the two thermocouples was measured as a function of time. The process was then repeated at the same temperature using the other heater. Typical raw data for such a single measurement (Figure 3a,b) show that the application of 2.0 W to H_1 produces a stepwise increase at both TC_1 and TC_2, but the increase at TC_1 is 0.60 K higher than that seen at TC_2, location 200 μm from TC1 (Figure 3a). This induced ΔT produces a V_s of -200 μV in the PdTe nanowire array (Figure 3b). The negative sign on V_s confirms that the majority of carriers in these nanowires are electrons. The two sets of measured values for V_s as a function of T (Figure 3d,e) correspond to the measurement of this quantity using the two heaters, using the indicated heater powers.

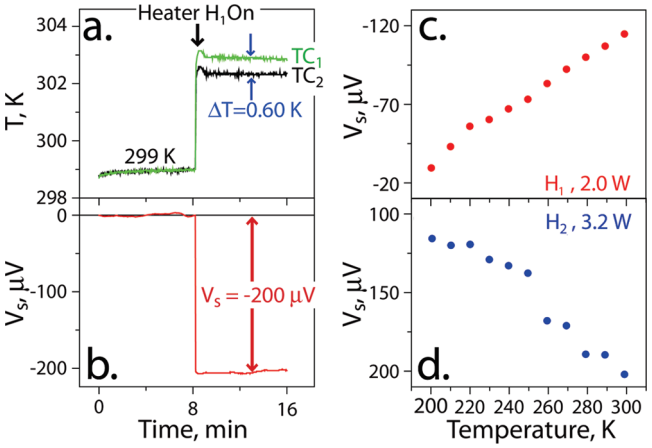

Figure 3. Raw data for the measurement of the Seebeck coefficient for an array of 250 unannealed 60 × 200 nm PbTe nanowires. (a) Thermocouple (TC_1 and TC_2) response before and after turning on heater 1 (H_1). (b) Seebeck voltage (V_s) response of -200 μV to the temperature gradient produced by powering H_1, as shown in (a). (c,d) Plots of the measured V_s versus T acquired for the use of the two heaters, producing temperature gradients along opposite directions of the PbTe nanowire array. The power applied to the two heaters is as indicated.

The magnitude of the measured S increases linearly with T for all four annealing temperatures, in accordance with the Mott equation[43,44]

$$S = \frac{2\pi^2 k^2 m^*}{3(3\pi^2)^{2/3}\hbar q n^{2/3}} T \qquad (2)$$

where k is Boltzman's constant, m^* is the effective mass of the electron, q is the elementary charge, and n is the carrier concentration. Using eq 2, the carrier concentration, n, can be estimated from the experimentally determined slope of S versus T from Figure 4a and the known effective mass of electrons in PbTe ($m^* = 0.25 m_0$[45]). This equation is valid for degenerate semiconductors having carrier concentrations in the range from 10^{18}–10^{20} cm^{-3}.[46,47] Upon the basis of our analysis of S versus T presented below, the dopant density for

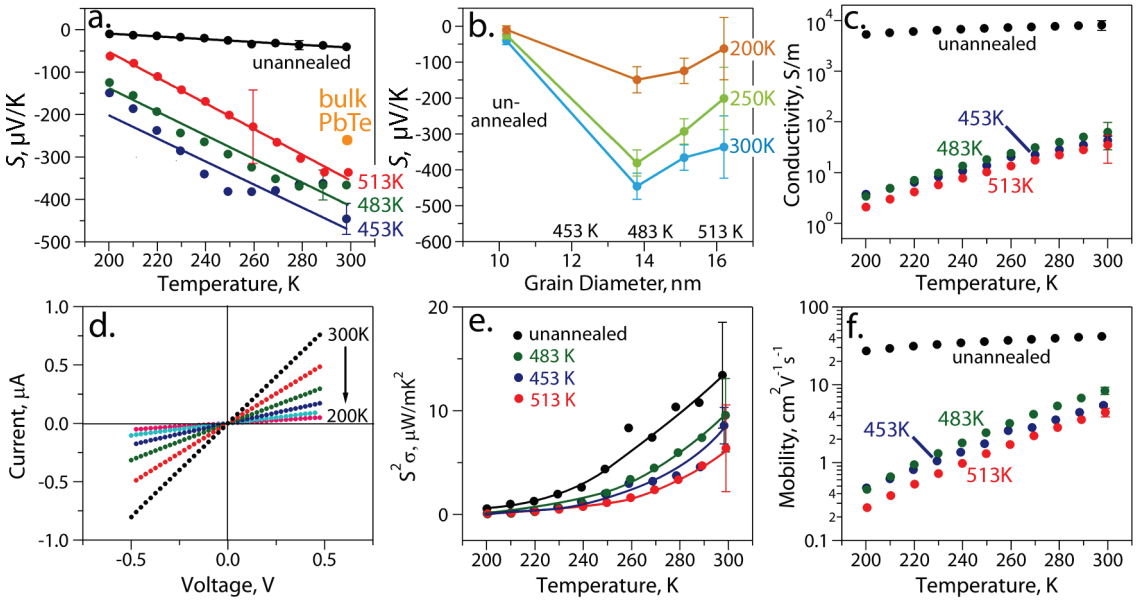

Figure 4. Influence of T_{anneal} on the S and σ of 60 × 200 nm PbTe nanowires. (a) Plots of Seebeck coefficient against annealing temperature, T_{anneal}, for PbTe nanowires that were unannealed (black) and for T_{anneal} = 453 (blue), 483 (green), and 513 K(red). For each temperature, values from three samples were averaged; error bars indicate $\pm 1\sigma$. Solid lines are least-squares fits to the data. (b) Plots of S, measured at three temperatures, as indicated, versus the mean grain diameter. (c) Plots of σ versus T for the same 12 samples measured in (a) and (b). (d) Typical current versus voltage curves obtained for an array of ~200 PbTe nanowires recorded as a function of T in the temperature window of 200–300 K. The linearity of these plots demonstrates that the nickel electrical contacts are ohmic. (e) The power factor, $S^2\sigma$, plotted against T_{anneal}. Error bars indicate $\pm 1\sigma$ for measurements conducted on three nanowire samples. (f) The carrier mobility versus temperature for unannealed PbTe nanowires and for those annealed at three temperatures, as indicated.

© 2010 American Chemical Society

DOI: 10.1021/jz101128d | J. Phys. Chem. Lett. 2010, 1, 3004–3011

the PbTe nanowires investigated here was at the lower end of this range, $0.47(\pm 0.07)-12(\pm 2) \times 10^{18}$ cm^{-3}.

For PbTe nanowires annealed at 453 K, we find that S (at 300K) is increased from -41 μV/K for unannealed wires to -479 μV/K, 80 % larger in magnitude than the S of bulk PbTe of -260 μV/K (Figure 4b).[48] The electrical conductivity was measured as follows. First, the conductance of the nanowire array between 200 and 300 K was measured immediately after measurement of the Seebeck coefficient without breaking vacuum. From this series of measurements, a temperature coefficient of conductance, TCC = dσ/dT, specific to these nanowires was obtained. Next, all of the nanowires between TC_1 and TC_2 except the orphaned nanowire (Figure 1) were cut manually using a glass capillary. Then, the electrical conductance of the orphaned nanowire was measured at 300 K by acquiring a current−voltage trace. The conductivity of this nanowire was then calculated from its SEM-measured width (W) and AFM-measured height (H) using $\sigma = (IL)/(VWH)$, where I is the current measured at a voltage V and L is the length of the nanowire between the electrical contacts. Values for σ at temperatures other than 300 K were obtained using the temperature coefficient of conductance measured for the nanowire array.

Thermal annealing at all three T_{anneal} values (Figure 4c) reduces σ by 2−3 orders of magnitude, and no significant variation of σ is seen over the range of T_{anneal} from 453 to 513 K (Figure 4c). This depression of σ results in a net reduction in the power factor, $S^2\sigma$, despite the elevation of S at the annealed nanowire samples (Figure 4e). Finally, using the measured values of σ and n, the electron mobility, μ, is obtained using the equation $\mu = \sigma/nq$ (Figure 4f).[48,49] Our measured μ values (Figure 4f) are much smaller than that of bulk PbTe (~1400 cm^2 V^{-1} s^{-1} [50]) but somewhat higher than the value of 0.7 cm^2 V^{-1} s^{-1} (300 K) measured by Yang and co-workers[23] for single-crystalline PbTe nanowires. Upon the basis of the XPS results presented above, we tentatively attribute the depression of μ caused by thermal annealing to enhanced boundary scattering of electrons induced by the oxide layer.[51]

Prior measurements of S and σ for PbTe are summarized in Table 1. Relative to our measurement of $S = -479$ μV/K (300 K) for PbTe nanowires annealed at 453 K, larger values of S have been reported in just one previous case by Guo et al.,[22] who found $S = -628$ μV/K for a film of single-crystalline, 30 nm diameter PbTe nanowires annealed at 353 K for 12 h. What is responsible for the huge Seebeck coefficient enhancement of these annealed PbTe nanowires? One can gain some insight from an alternative form of the Mott equation[46]

$$S = \frac{2\pi^2 k^2}{3q}\left\{\frac{1}{n}\frac{dn(E)}{dE} + \frac{1}{\mu}\frac{d\mu(E)}{dE}\right\} \qquad (3)$$

where $n(E)$ and $\mu(E)$ are the energy-dependant carrier concentration and carrier mobility, respectively, and q is the elementary charge. Equation 3 predicts that an elevation of S can be associated with a decrease in n and/or μ, both of which we have observed here (Figure 4f, Table 1), but we are unable to estimate the values of d$n(E)$/dE and d$\mu(E)$/dE and therefore to predict S using our measured values of n without additional information.

In summary, a new approach for measuring S and σ for nanowires involves the fabrication of electrical contacts on top of a lithographically patterned array of nanowires, prepared using the LPNE method. At an optimum annealing temperature of 453 K, the S at 300 K is increased from -41 μV/K for unannealed wires to -479 μV/K, 80 % larger in magnitude than the S (-260 μV/K) of bulk PbTe. In future work, the surface oxidation of these PbTe nanowires during the annealing process must be suppressed in order to achieve higher carrier mobilities, leading to higher electrical conductivities and enhanced power factors.

AUTHOR INFORMATION

Corresponding Author:

*To whom correspondence should be addressed. E-mail: rmpenner@uci.edu.

ACKNOWLEDGMENT This work was supported by the National Science Foundation Grant DMR-0654055, and the UCI School of Physical Sciences Center for Solar Energy. J.C.H. and M.C. acknowledge funding from the DOE Office of Basic Energy Sciences (DE-FG02-96ER45576).

REFERENCES

(1) Rowe, D. M. *CRC Handbook of Thermoelectrics: From Micro to Nano*; CRC Press: Boca Raton, FL, 2006.
(2) Rogach, A. L.; Eychmueller, A.; Hickey, S. G.; Kershaw, S. V. Infrared-Emitting Colloidal Nanocrystals: Synthesis, Assembly, Spectroscopy, and Applications. *Small* **2007,** *3*, 536–557.
(3) Murphy, J.; Beard, M.; Norman, A.; Ahrenkiel, S.; Johnson, J.; Yu, P.; Micic, O.; Ellingson, R.; Nozik, A. PbTe Colloidal Nanocrystals: Synthesis, Characterization, and Multiple Exciton Generation. *J. Am. Chem. Soc.* **2006,** *128*, 3241–3247.
(4) Goldsmid, H. J. *Electronic Refrigeration*; Pion: London, 1986.
(5) Hicks, L.; Dresselhaus, M. Thermoelectic Figure of Merit of a One-Dimensionsal Conductor. *Phys. Rev. B* **1993,** *47*, 16631–16634.
(6) Hicks, L.; Dresselhaus, M. Effect of Quantum-Well Structures on the Thermoelectric Figure of Merit. *Phys. Rev. B* **1993,** *47*, 12727–12731.
(7) Balandin, A.; Wang, K. Effect of Phonon Confinement on the Thermoelectric Figure of Merit of Quantum Wells. *J. Appl. Phys.* **1998,** *84*, 6149–6153.
(8) Balandin, A.; Wang, K. Significant Decrease of the Lattice Thermal Conductivity Due to Phonon Confinement in a Free-Standing Semiconductor Quantum Well. *Phys. Rev. B* **1998,** *58*, 1544–1549.
(9) Zou, J.; Balandin, A. Phonon heat Conduction in a Semiconductor Nanowire. *J. Appl. Phys.* **2001,** *89*, 2932–2938.
(10) Walkauskas, S.; Broido, D.; Kempa, K.; Reinecke, T. Lattice Thermal Conductivity of Wires. *J. Appl. Phys.* **1999,** *85*, 2579–2582.
(11) Zhou, J.; Jin, C.; Seol, J.; Li, X.; Shi, L. Thermoelectric Properties of Individual Electrodeposited Bismuth Telluride Nanowires. *Appl. Phys. Lett.* **2005,** *87*, 133109.
(12) Mavrokefalos, A.; Moore, A. L.; Pettes, M. T.; Shi, L.; Wang, W.; Li, X. Thermoelectric and Structural Characterizations of Individual Electrodeposited Bismuth Telluride Nanowires. *J. Appl. Phys.* **2009,** *105*, 104318.
(13) Seol, J. H.; Moore, A. L.; Saha, S. K.; Zhou, F.; Shi, L.; Ye, Q. L.; Scheffler, R.; Mingo, N.; Yamada, T. Measurement and

© 2010 American Chemical Society

DOI: 10.1021/jz101128d | *J. Phys. Chem. Lett.* **2010,** *1*, 3004–3011

Analysis of Thermopower and Electrical Conductivity of an Indium Antimonide Nanowire From a Vapor−Liquid−Solid Method. *J. Appl. Phys.* **2007,** *101*, 023706.

(14) Zhou, F.; Seol, J. H.; Moore, A. L.; Shi, L.; Ye, Q. L.; Scheffler, R. One-Dimensional Electron Transport and Thermopower in an Individual InSb Nanowire. *J. Phys.: Condens. Matter* **2006,** *18*, 9651–9657.

(15) Zhou, F.; Moore, A. L.; Pettes, M. T.; Lee, Y.; Seol, J. H.; Ye, Q. L.; Rabenberg, L.; Shi, L. Effect of Growth Base Pressure on the Thermoelectric Properties of Indium Anti-monide Nanowires. *J. Phys. D: Appl. Phys.* **2010,** *43*, 025406.

(16) Jang, S. Y.; Kim, H. S.; Park, J.; Jung, M.; Kim, J.; Lee, S. H.; Roh, J. W.; Lee, W. Transport Properties of Single-Crystalline n-Type Semiconducting PbTe Nanowires. *Nanotechnol.* **2009,** *20*, 415204.

(17) Roh, J. W.; Jang, S. Y.; Kang, J.; Lee, S.; Noh, J.-S.; Kim, W.; Park, J.; Lee, W. Size-Dependent Thermal Conductivity of Individual Single-Crystalline PbTe Nanowires. *Appl. Phys. Lett.* **2010,** *96*, 103101.

(18) Hochbaum, A. I.; Chen, R.; Delgado, R. D.; Liang, W.; Garnett, E. C.; Najarian, M.; Majumdar, A.; Yang, P. Enhanced Thermoelectric Performance of Rough Silicon Nanowires. *Nature* **2008,** *451*, 163–168.

(19) Boukai, A. I.; Bunimovich, Y.; Tahir-Kheli, J.; Yu, J.-K.; Goddard, I.; William, A.; Heath, J. R. Silicon Nanowires As Efficient Thermoelectric Materials. *Nature* **2008,** *451*, 168–171.

(20) Zhang, L.; Yu, J.; Mo, M.; Wu, L.; Kwong, K.; Li, Q. A General In Situ Hydrothermal Rolling-Up Formation of One-Dimensional, Single-Crystalline Lead Telluride Nanostructures. *Small* **2005,** *1*, 349–354.

(21) Tai, G.; Guo, W.; Zhang, Z. Hydrothermal Synthesis and Thermoelectric Transport Properties of Uniform Single-Crystalline Pearl-Necklace-Shaped PbTe Nanowires. *Cryst. Growth Des.* **2008,** *8*, 2906–2911.

(22) Tai, G.; Zhou, B.; Guo, W. Structural Characterization and Thermoelectric Transport Properties of Uniform Single-Crystalline Lead Telluride Nanowires. *J. Phys. Chem. C* **2008,** *112*, 11314–11318.

(23) Fardy, M.; Hochbaum, A. I.; Goldberger, J.; Zhang, M. M.; Yang, P. Synthesis and Thermoelectrical Characterization of Lead Chalcogenide Nanowires. *Adv. Mater.* **2007,** *19*, 3047–3051.

(24) Harman, T.; Reeder, R.; Walsh, M.; LaForge, B.; Hoyt, C.; Turner, G. High Electrical Power Density from PbTe-Based Quantum-Dot Superlattice Unicouple Thermoelectric Devices. *Appl. Phys. Lett.* **2006,** *88*, 243504.

(25) Harman, T.; Taylor, P.; Walsh, M.; LaForge, B. Quantum Dot Superlattice Thermoelectric Materials and Devices. *Science* **2002,** *297*, 2229–2232.

(26) Liu, W.; Cai, W.; Yao, L. Electrochemical Deposition of Well-Ordered Single-Crystal PbTe Nanowire Arrays. *Chem. Lett.* **2007,** *36*, 1362–1363.

(27) Saloniemi, H.; Kemell, M.; Ritala, P.; Leskela, M. PbTe Electrodeposition Studied by Combined Electrochemical Quartz Crystal Microbalance and Cyclic Voltammetry. *J. Electroanal. Chem.* **2000,** *482*, 139–148.

(28) Sima, M.; Enculescu, I.; Sima, M.; Vasile, E. Semiconductor Nanowires Obtained by Template Method. *J. Optoelectron. Adv. Mater.* **2007,** *9*, 1551–1554.

(29) Sima, M.; Enculescu, I.; Vasile, E. Growth of ZnO Micro and Nanowires Using the Template Method. *J. Optoelectron. Adv. Mater.* **2006,** *8*, 825–828.

(30) Yang, Y.; Taggart, D. K.; Brown, M. A.; Xiang, C.; Kung, S.-C.; Yang, F.; Hemminger, J. C.; Penner, R. M. Wafer-Scale Patterning of Lead Telluride Nanowires: Structure, Characteriza-tion, and Electrical Properties. *ACS Nano* **2009,** *3*, 4144–4154.

(31) Yang, Y.; Kung, S. C.; Taggart, D. K.; Xiang, C.; Yang, F.; Brown, M. A.; Guell, A. G.; Kruse, T. J.; Hemminger, J. C.; Penner, R. M. Synthesis of PbTe Nanowire Arrays Using Lithographically Patterned Nanowire Electrodeposition. *Nano Lett.* **2008,** *8*, 2447–2451.

(32) Patterson, A. L. The Scherrer Formula for X-ray Particle Size Determination. *Phys. Rev.* **1939,** *56*, 978–982.

(33) Wagner, C.; Naumkin, A.; Kraut-Vass, A.; Allison, J.; Powell, C.; Rumble, J. J. *NIST X-ray Photoelectron Spectroscopy Database.* http://srdata.nist.gov/xps/ (accessed June 1, 2010).

(34) Yashina, L.; Tikhonov, E.; Neudachina, V.; Zyubina, T.; Chaika, A.; Shtanov, V.; Kobeleva, S.; Dobrovolsky, Y. The Oxidation of PbTe(100) Surface in Dry Oxygen. *Surf. Interface Anal.* **2004,** *36*, 993–996.

(35) Green, M.; Lee, M. Interaction of Oxygen with Clean Lead Telluride Surfaces. *J. Phys. Chem. Solids* **1966,** *27*, 796–804.

(36) Taylor, J. A.; Perry, D. L. An X-Ray Photoelectron and Electron-Energy Loss Study of the oxidation of Lead. *J. Vac. Sci. Technol., A* **1984,** *2*, 771–774.

(37) Nefedov, V. X-ray Photoelectron Study of Surface Compounds Formed During Flotation of Minerals. *Surf. Interface Anal.* **1980,** *2*, 170–172.

(38) Marra, W. C.; Eisenberger, P.; Cho, A. Y. X-Ray Total-External-Reflection-Bragg Diffraction — Stuctural Study of the GAAS−Al Interface. *J. Appl. Phys.* **1979,** *50*, 6927–6933.

(39) Bando, H.; Koizumi, K.; Oikawa, Y.; Daikohara, K.; Kulbachinskii, V. A.; Ozaki, H. The Time-Dependent Process of Oxidation of the Surface of Bi_2Te_3 Studied by x-ray Photoelectron Spectroscopy. *J. Phys.: Condens. Matter* **2000,** *12*, 5607–5616.

(40) Powell, C. J.; Jablonski, A. *NIST Electron Inelastic-Mean-Free-Path Database, Version 1*,1st ed.; National Institute of Standards and Technology: Washington, DC, 2000.

(41) Sun, T.; Byer, N.; Chen, J. Oxygen-Uptake on Epitaxial PbTe-(111) Surfaces. *J. Vac. Sci. Technol.* **1978,** *15*, 585–589.

(42) Bettini, M.; Richter, H. Oxidation in Air and Thermal Desorption on PbTe, SnTe, and $Pb_{0.8}Snthia_{0.2}Te$ Surfaces. *Surf. Sci.* **1979,** *80*, 334–343.

(43) Cutler, M.; Leavy, J. F.; Fitzpatrick, R. L. Electronic Transport in Semimetallic Cerium Sulfide. *Phys. Rev. A* **1964,** *133*, 1143–1152.

(44) Snyder, G. J.; Toberer, E. S. Complex Thermoelectric Materials. *Nat. Mater.* **2008,** *7*, 105–114.

(45) Lyden, H. A. Temperature Dependence of Effective Masses in PbTe. *Phys. Rev. A* **1964,** *135*, A514–A521.

(46) Heremans, J. P.; Jovovic, V.; Toberer, E. S.; Saramat, A.; Kurosaki, K.; Charoenphakdee, A.; Yamanaka, S.; Snyder, G. J. Enhancement of Thermoelectric Efficiency in PbTe by Distortion of the Electronic Density of States. *Science* **2008,** *321*, 554–557.

(47) Lee, C. H.; Yi, G. C.; Zuev, Y. M.; Kim, P. Thermoelectric Power Measurements of Wide Band Gap Semiconducting Nanowires. *Appl. Phys. Lett.* **2009,** *94*, 022106.

(48) Heremans, J.; Thrush, C.; Morelli, D. Thermopower Enhancement in PbTe With Pb Precipitates. *J. Appl. Phys.* **2005,** *98*, 063703.

(49) Wang, R. Y.; Feser, J. P.; Lee, J. S.; Talapin, D. V.; Segalman, R.; Majumdar, A. Enhanced Thermopower in PbSe Nanocrystal Quantum Dot Superlattices. *Nano Lett.* **2008,** *8*, 2283–2288.

(50) Thiagarajan, S. J.; Jovovic, V.; Heremans, J. P. On the Enhancement of the Figure of Merit in Bulk Nanocomposites. *Phys. Status Solidi* **2007,** *1*, 256–258.

© 2010 American Chemical Society

DOI: 10.1021/jz101128d | *J. Phys. Chem. Lett.* **2010,** *1*, 3004–3011

(51) Ito, M.; Seo, W. S.; Koumoto, K. Thermoelectric Properties of PbTe Thin Films Prepared by Gas Evaporation Method. *J. Mater. Res.* **1999,** *14*, 209–212.
(52) Yan, Q.; Chen, H.; Zhou, W.; Hng, H. H.; Boey, F. Y. C.; Ma, J. A Simple Chemical Approach for PbTe Nanowires with Enhanced Thermoelectric Properties. *Chem. Mater.* **2008,** *20*, 6298–6300.
(53) Purkayastha, A.; Yan, Q.; Gandhi, D. D.; Li, H.; Pattanaik, G.; Borca-Tasciuc, T.; Rav- ishankar, N.; Ramanath, G. Sequential Organic−Inorganic Templating and Thermoelectric Properties of High-Aspect-Ratio Single-Crystal Lead Telluride Nanorods. *Chem. Mater.* **2008,** *20*, 4791–4793.
(54) Wan, B.; Hu, C.; Xi, Y.; Xu, J.; He, X. Room-Temperature Synthesis and Seebeck Effect of Lead Chalcogenide Nanocubes. *Solid State Sci.* **2010,** *12*, 123–127.
(55) Heremans, J.; Thrush, C.; Morelli, D. Thermopower Enhancement in Lead Telluride Nanostructures. *Phys. Rev. B* **2004,** *70*, 5–12.

© 2010 American Chemical Society

DOI: 10.1021/jz101128d | *J. Phys. Chem. Lett.* **2010,** *1*, 3004–3011